Interfacial Coulomb-enhanced charge injection for efficient perovskite light-emitting diodes

Yongjian Chen [a], Cheng Yan [a,d,**], Zhenyu Chen [a], Xiankan Zeng [a], Qungui Wang [c], Shiyu Yang [a], Lunyao Pan [a], Chenglong Li [a], Maolin Mu [a], Wen Li [a,1], Guanqi Tang [b,***], Weiqing Yang [a,b,*]

[a] Key Laboratory of Advanced Technologies of Materials (Ministry of Education), School of Materials Science and Engineering, Southwest Jiaotong University, Chengdu, 610031, PR China
[b] Research Institute of Frontier Science, Southwest Jiaotong University, Chengdu, 610031, PR China
[c] College of Physics, Sichuan University, Chengdu, 610065, PR China
[d] Institute of Fundamental and Frontier Sciences, University of Electronic Science and Technology of China, Chengdu, 611731, PR China

A B S T R A C T

Unbalanced electron-hole injection in perovskite light-emitting diodes (PeLEDs) has always been a major stumbling block limiting device performance. Here we develop a heterointerface Coulomb enhancement strategy to efficiently promote electron injection between perovskite emitter and transport layer and thereby balance the electron-hole recombination equilibrium through manipulating defect-rich positive-charge centers induced Coulomb interactions in LiF interlayer. Through multiscale polarization response characterizations combined with capacitance-voltage and electrochemical impedance spectroscopy, it is confirmed that diffusing holes trapped in LiF layer leads to the increased interfacial polarization. Moreover, the polarization response reversal and high-frequency-dependent dissipation sensitivity further corroborate the LiF-induced interfacial Coulomb enhancement mechanism. The universality of the concept is also successfully verified in devices with electron-only, hole-only, and PN structures. Consequently, the modified PeLEDs show a lower leakage current, along with a significant performance improvement by 1.9 times in external quantum efficiency (18.8%) and 5.7 times in luminance compared with control samples. This study provides a unique perspective to promote carrier transport balance by taking advantage of physical effects within interlayer.

1. Introduction

Benefitting from the comprehensively excellent photoelectric properties of metal halide perovskite materials, such as high photoluminescence quantum yields (PLQY), high color purity, high carrier mobility, tunable bandgap, and ease of fabrication [1–8], etc., perovskite light-emitting diodes hold great promise in fields such as ultra-high-definition displays and solid-state lighting [9–15]. Since the realization of room-temperature perovskite luminescence in 2014 [16], numerous researchers have dedicated their efforts to advancing the PeLEDs technology. Recently, significant breakthroughs have been achieved with the highest external quantum efficiency in PeLEDs, surpassing 20% for blue [11], 30% for green [17], and 20% for red [12]. However, the presence of intrinsic defects in perovskite materials leads to low PLQY and non-radiative recombination [18], imbalanced carrier injection, and low injection efficiency [19], which still poses significant

challenges in fabricating high-performance PeLEDs and realizing further commercialization.

Balanced carrier injection is highly critical to obtaining high-performance PeLEDs since unbalanced recombination would lead to charge accumulation and exciton quenching, resulting in low device efficiency and stability [20–23] [20–23] [20–23]. Interface engineering and energy level regulation are effective means to solve this problem. For example, charge transport layer (CTL) with relatively matched energy levels is introduced to reduce the charge accumulation between CTL and emissive layer (EML) [24–27] [24–27] [24–27]. Functional interface layers, such as perfluorinated ionomer film [28], electric dipole layer [29], nickel acetate layer [30], etc., are also introduced to balance carrier injection and improve device performance. However, designing a suitable CTL with a well-aligned energy level that facilitates charge transport is still challenging [31]. Therefore, it is desirable to develop more efficient means to balance the carrier injection, thereby

improving the performance of PeLEDs.

In this work, a novel strategy is demonstrated to enhance electron injection by introducing a functional interface layer where defects can induce the formation of positive charge centers between EML and electron transport layer (ETL) to attract electrons based on Coulomb interactions. Specifically, a thermally evaporated thin LiF film featured with high defect density is employed as the Coulomb-enhanced interlayer, and defects are further generated under electric field. These defects will trap holes diffusing from the EML during the carrier diffusion stage of electroluminescence process and convert to defect-positive charge centers, whose Coulombic interactions with electrons from ETL will further facilitate electron injection. The processes of holes trapping by defects, electron injection enhanced by Coulomb interactions and carrier accumulation reduction have been confirmed by multiscale polarization response characterizations combined with capacitance-voltage and electrochemical impedance spectroscopy. Interestingly, although these defects in LiF film lead to non-radiative recombination and PL quenching, the enhanced charge injection and balanced carrier recombination lead to less energy loss and an improvement in electroluminescence performance and stability. Ultimately, the peak EQE is increased from 9.9% to 18.8%, and luminance is substantially enhanced from 14379 cd/m^2 to 82743 cd/m^2. Simultaneously, we further validate the universality of this concept in single-carrier devices, PN-type devices, and PeLEDs prepared from perovskite nanocrystals with different composition. This study dexterously takes advantage of defects that are generally considered to be detrimental to improve the performance of PeLEDs by enhancing charge injection, demonstrating a new perspective on device design based on physical effects in the interface layer.

2. Experimental section

2.1. Materials

Lead bromide (PbBr$_2$, 99%) and n-diacylamine (98%) were obtained from Shanghai Macklin Co., Ltd., Keshi provided ethanol, *N,N*-Dimethylformamide (DMF, 98%), 1-butanol (98%), n-hexane (98%), n-Octane (99%) and toluene (99.9%). Additionally, oleic acid (OA, 90%), molybdenum trioxide (MoO$_3$, 99.95%), LiF, and chlorobenzene (98%) were sourced from Shanghai Aladdin Industrial Corporation Co., Ltd. Xi'an Yuri solar Corp supplied Poly(3,4-ethylenedioxythiophene) polystyrene sulfonate (PEDOT:PSS), poly(9-vinylcarbazole) (PVK), 4,6-bis (3,5-di(pyridin-3-yl)phenyl)-2-methylpyrimidine (B$_3$PyMpM),formamidine bromide (FABr), guanidinium bromide (GABr), Tris(4-carbazoyl-9-ylphenyl)amine (TCTA), phenethylammonium bromide (PEABr). Lastly, Guangdong Poly Optoelectronics Co. Ltd supplied ZnMgO. No further purifications of any materials were required before use.

2.2. Preparation of perovskite nanocrystals

FA$_{0.85}$GA$_{0.15}$PbBr$_3$ precursor (170 μL), prepared by dissolving FABr, GABr, and PbBr$_2$ in DMF with a molar ratio of 7:1:4 and Pb^{2+} concentration at 0.2 M, was injected into a vial containing a crystallization-inducing solution composed of 5 mL of toluene, 2 mL of 1-butanol, 350 μL of oleic acid, and 28 μL of n-diacylamine. The solution was vigorously stirred for 10 min after the injection, following which it was centrifuged at 13000 rpm for 5 min and the supernatant was discarded. The precipitate was redispersed in 1 mL of a mixture of n-hexane and n-octane in a 1:2 vol ratio and then centrifuged at 2500 rpm for 2 min. The resulting supernatant was filtered through a 0.22 μm PTFE filter to collect FA$_{0.85}$GA$_{0.15}$PbBr$_3$ NCs. FAPbBr$_3$ precursor (170 μL) was prepared by dissolving FABr and PbBr$_2$ in DMF with a molar ratio of 2:1 and Pb^{2+} concentration at 0.2 M FA$_{0.8}$GA$_{0.1}$PEA$_{0.1}$PbBr$_3$ precursor (170 μL) was prepared by dissolving FABr, GABr, PEABr and PbBr$_2$ in DMF with a molar ratio of 8:1:1:5 and Pb^{2+}concentration at 0.2 M. The ambient temperature was about 25 °C.

2.3. Device fabrication

The devices were fabricated according to our previous report with some modifications. Indium tin oxide (ITO) patterned glasses were cleaned sequentially by sonication with optical glass cleaning agent, deionized water, acetone, isopropanol and ethanol for 15 min each, then blow-dried using a nitrogen gun, and then transferred into an ultraviolet-ozone cleaner treated for 30 min to remove the residual organics and dangling bond. Following the PEDOT:PSS was spin-coated on the substrate at 3000 rpm for 30 s. After annealed at 150 °C for 15 min, the PEDOT:PSS was transferred into a N$_2$-glove box. After cooled down to room-temperature, the PVK, at a concentration of 4 mg/mL in chlorobenzene, was then spin-coated at 4000 rpm for 40 s. The PVK film was annealed at 160 °C for 20 min. Perovskite NCs were subsequently spin-coated at 1000 rpm for 40 s and then quickly transferred into a high-vacuum evaporator without annealing. Afterward, in a low-vacuum environment of 8 × 10^{-5}Pa, a sequential deposition of 1 nm or 8 nm LiF (this step was not present in control group),40 nm of B$_3$PyMpM, 1 nm of LiF, and 80 nm of Al was carried out. The hole-only device was fabricated by sequentially deposit 30 nm TCTA, 3 nm of MoO$_3$ and 80 nm of Ag onto perovskite film with or without LiF. The electron-only device was fabricated by replacing the PEDOT: PSS/PVK to ZnMgO film. And the ZnMgO film was made by spin-coated ZnMgO (20 mg/mL in ethanol) at 4000 rpm for 40 s on the ultraviolet-ozone treated ITO and annealed at 120 °C for 10 min. The evaporation rates of B$_3$PyMpM, LiF, Al, TCTA, MoO$_3$ and Ag were 0.3, 0.1, 1.5, 0.3, 0.1 and 1.5 Å s^{-1}, respectively. The emissive area of the devices was 4 mm^2 (2 mm × 2 mm), which was defined by the overlapping area between the ITO and Al electrodes.

2.4. Characteristics

The photoluminescence spectra (PL) spectra were measured by FLS 980 (Edinburgh Instruments) spectrometer with a 450 W Xenon lamp. Time-resolved PL spectra were characterized by picosecond pulsed diode laser coupled with a time-corrected single-photon counting system (TCSPC) of Edinburgh instruments. The C–V, multiscale capacitance/polarization response (AC signal amplitude is 30 mV), and reactance tests of PeLEDs, current density-voltage curves of single carrier and PN-type devices were performed by Keithley 4200. All the EIS tests were carried out by the multichannel Squidstat Solo and Squidstat Plus. The Keithley 2400 source meter combined with a QE-Pro spectrometer (Ocean Optics), were employed to characterize the performances of PeLEDs in glove box. FTIR spectra were performed by Bruker Invneio S.

3. Results and discussion

3.1. The effect of LiF Coulomb-enhanced interlayer on interfacial charge injection and accumulation

Fig. 1a demonstrates the mechanism of enhanced charge injection mediated by the LiF Coulomb-enhanced interlayer (CEI). The LiF film formed by thermal evaporation exhibits a notably high defect density. In addition, under the influence of electric field, point defects of isolated F-centers as well as more complex defects formed by F-aggregation, such as F$_2$, F$_3^-$, etc. [32] are generated simultaneously. These defects serve as defect-positive charge centers by trapping diffusing holes and further enhancing charge injection through Coulomb interactions with electrons, facilitating carrier injection equilibrium and reducing interfacial charge accumulation.

3.2. Defects trapping of diffusing holes and formation of defect-positive charge centers within LiF

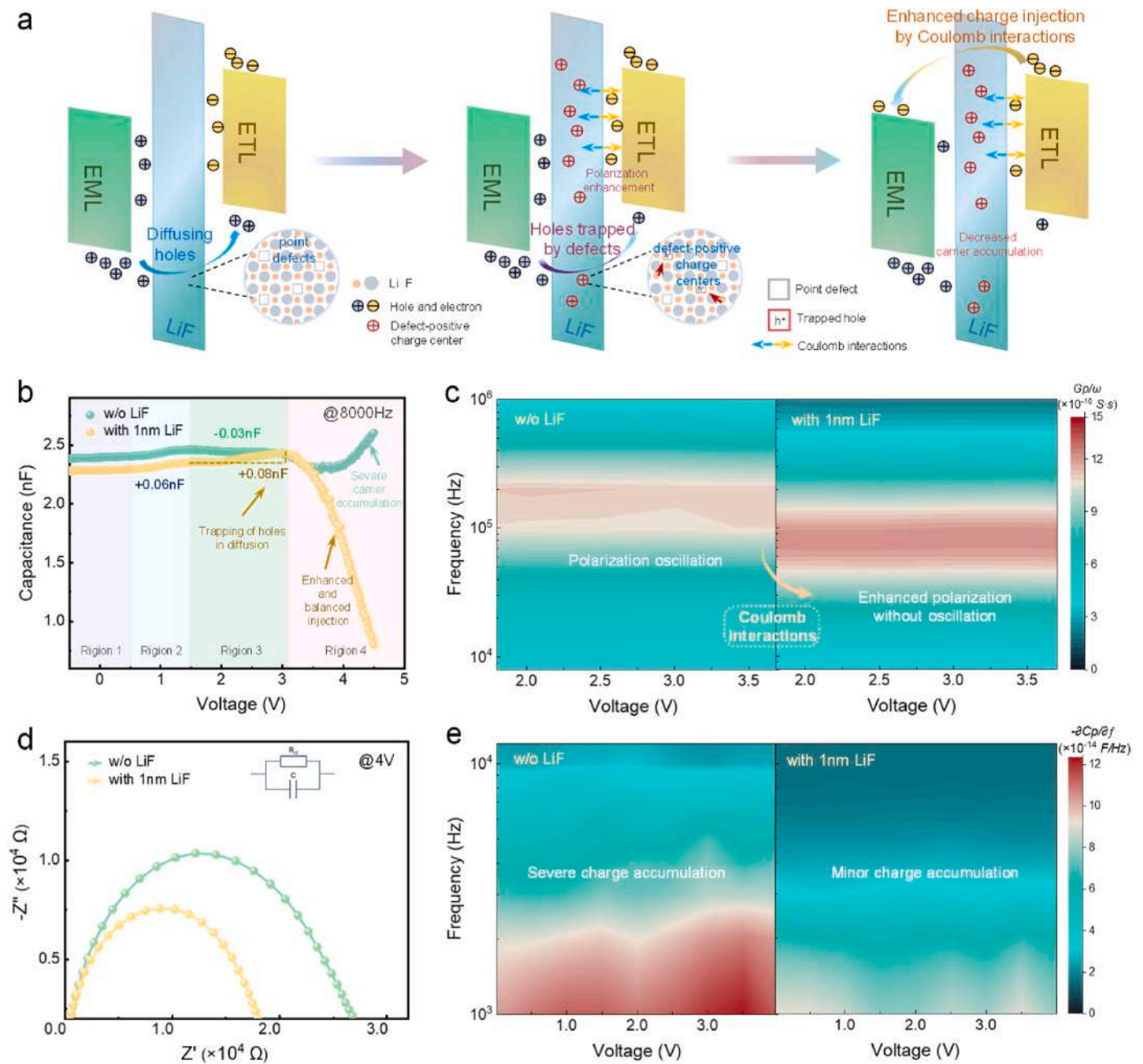Multiscale capacitance/polarization response testing is a frequency-

Fig. 1. (a) The schematic diagram of charge injection mechanism enhanced by LiF Coulomb-enhanced interlayer. (b) C–V plots, (c) multiscale polarization response, (d) Nyquist plots, and (e) multiscale capacitance response of PeLEDs without and with LiF Coulomb-enhanced interlayer.

domain dependent method to study the interfacial electro-polarization and carrier accumulation of LED devices [33]. Generally, the capacitance-voltage (C–V) characteristics quantitatively measure changes in space charge within the device and describe carrier behavior, and the capture of holes by defects in LiF can be observed during the diffusion stage of electroluminescence process. In cases where the PeLEDs emission is sufficiently intense, and the injection barrier is relatively low, an ideal C–V curve can be divided into four regions, and each region corresponds to a capacitance, C_1, C_2, C_3, and C_4, representing geometric capacitance, barrier capacitance, diffusion capacitance, and the sum of the charge injection and consumption, respectively [34]. As shown in Fig. 1b, the C–V characteristics of PeLEDs (The structure is shown in Fig. S1) can be similarly partitioned into four distinct regions. In region 2, it is observed that the introduction of LiF interlayer does not induce any discernible alteration in C_2 (both C_2 are

+0.03 nF), which implies that LiF does not result in a change in the accumulation of interfacial charge carriers at low voltages. However, a marked discrepancy emerges in region 3. C_3, representing the diffusion capacitance, primarily delineates the profound influence of major charge carriers (holes) during the transport on the capacitance. In the control system, C_3 is -0.03 nF. This negative value suggests the recombination of holes migrating from EML to ETL at the interface. Following the introduction of 1 nm LiF interlayer, C_3 becomes $+0.08$ nF, which implies that holes, during diffusion stage from EML to ETL, are trapped by the defects in LiF film.

Predictably, the defects in LiF would lead to a change in electro-polarization of the system after trapping diffusing holes, we employ the ratio of conductivity to angular frequency (Gp/ω) to analyze the electro-polarization degree of PeLEDs under the influence of electric field [35]. As shown in Fig. 1c, in original system, the polarization

degree is high in the band of 10^5 to 2×10^5 Hz, and the polarization degree reaches the maximum at 2×10^5 Hz, and Gp/ω is 1.14×10^{-9} S s. Meanwhile, it is worth noting that the degree of polarization in the 10^5 to 2×10^5 Hz frequency band is accompanied by oscillation with voltage changes, which implies the continuous accumulation and recombination of interfacial carriers, agreeing with the analysis in C–V characteristics. In comparison, the polarization degree is enhanced with the Gp/ω increasing to 1.23×10^{-9} S s at 8×10^4 Hz after the introduction of LiF CEI, which is attributed to the trapping of diffusing holes causing the intensified asymmetry of positive and negative charge centers between CEI and ETL. Meanwhile, the oscillation phenomenon is weakened because of the inhibition of interfacial carrier accumulation and recombination between ETL and EML.

3.3. Coulomb interactions between defect-positive charge centers and electrons lead to enhanced charge injection and reduced carrier accumulation

Electrochemical impedance spectroscopy (EIS) is an electrochemical measurement method that applies small perturbations (current/voltage) to the system. Its significance has become increasingly prominent in recent years and is being utilized more frequently in research within the field of PeLEDs [36–38] [36–38] [36–38]. In the experiment, a small-amplitude AC voltage signal generates additional charge carriers, and the behavior of charge carriers is modulated by the spatial electric field formed by the DC bias voltage [39,40]. Nyquist plot, the portion near the origin is generated at high frequency, primarily stemming from impedance induced by charge transfer and the diameter of the circular arc can qualitatively describe the magnitude of impedance in different system [41,42]. When the Nyquist plot presents as a simple semicircle, we can adopt an equivalent circuit diagram, as illustrated in Fig. S2. As shown in Fig. 1d, the original system has R_{ct} of 1.34×10^4 Ω at a DC voltage of 4 V. Because of the Coulomb interactions between the defect-positive charge centers and electrons, the R_{ct} changes to 8.83×10^3 Ω after introducing 1 nm LiF CEI, implying that the Coulomb interactions lead to enhanced charge injection. The LiF interlayer also leads to a reduced accumulation of interfacial carriers. In the case where the whole system is analyzed as a circuit with a capacitor and a resistor in series (Fig. S3), the imaginary part of the capacitance (C'') decreases from the initial value of 1.6×10^{-6} F to 6.7×10^{-7} F when the frequency is 12 Hz (Fig. S4). Combined with the multiscale capacitance response, as shown in Fig. 1e, the initial system exhibits the deepest color within the frequency range of $<2 \times 10^4$ Hz, indicating a highest responsiveness of the system capacitance to frequency changes. However, the LiF interlayer attenuates this response from an initial maximum response value of 1.2×10^{-13} F/f to 8.9×10^{-14} F/f, which in combination with the reduction of reactance at different voltages after the introduction of LiF CEI, implying a reduction of capacitive component (Fig. S5). In addition, the decrease in C'' at low frequency evidence shows the reduction of carrier accumulation by defect-captured diffusing holes as well as Coulomb interactions-enhanced electron injection.

The effect of LiF CEI on the enhanced charge injection through Coulomb interactions and the reduction carrier accumulation in the luminescence process can be observed more directly in the region 4 of C–V curves (Fig. 1b). The trend of capacitance change simultaneously depends on the charge injection and consumption, and the capacitance varies with voltage to satisfy equation: $C = \frac{dQ}{dV} = \frac{dQ_{in} + dQ_{trap} - dQ_r}{dV}$, where Q_{in}, Q_{trap} and Q_r represents the total charge generated by injected carriers, trapped carriers, and recombined carriers (including radiative and non-radiative recombination) due to small-amplitude AC signal, respectively. During the initial stage of region 4, charge carriers recombining within the EML, with the increase of Q_r, the capacitance in the control group decreases as the voltage increases. As the voltage further increases, a phenomenon of capacitance stagnation followed by an increase occurs due to the increased Q_{in}. However, due to the enhanced charge injection with reduced carrier accumulation caused by LiF interlayer, the capacitance monotonically decreases with increasing voltage, which means stronger recombination with more balanced injection.

3.4. Further validation of the concept

Since the co-occurrence of carrier injection and recombination process increases the difficulty of analysis, and in order to further validate the concept that the defects in LiF interlayer capture holes to form defect-positive charge centers and enhance charge injection through Coulomb interactions, we decouple the devices and validate the concept in both single-carrier and PN-type devices.

Fig. 2a–d, and g represent the structure and carrier transport schematics of electron-only, hole-only and PN-type devices, respectively. In electron (hole)-only devices, the charge transport layer ideally provides sufficient shielding for holes (electrons). In such cases, it can be speculated that after the introduction of LiF CEI on perovskite in hole-only devices, the defects in LiF film will capture the holes and block the hole transport; similarly, in electron-only devices, there are no Coulomb interactions between LiF film and electrons due to the absence of defect-positive charge centers, and the electron transport is blocked by the dielectric properties of LiF film only. As shown in Fig. 2b–e, after the introduction of LiF interlayer in single-carrier devices, the current density decreased, and combined with its Nyquist plots at different voltages in Fig. 2c–f, it can be found that LiF interlayer hampers the carrier transport in the single-carrier devices, just as we have hypothesized.

Besides, since the surface ligands of perovskite nanocrystals can severely affect the charge injection [43], in order to exclude the possibility of reaction between LiF and the ligands and thus a change in carrier behavior, we conduct Fourier transform infrared spectra (FTIR) after depositing LiF film on perovskite. As shown in Fig. S6, LiF does not cause a shift in the characteristic peaks of –COOH and –NH$_2$ in oleic acid and decylamine. In PN-type devices where both holes and electrons coexist and also form defect-positive charge centers, 1 nm LiF CEI between PVK and B$_3$PyMpM leads to enhanced charge injection due to Coulomb interactions while excluding possible reactions between LiF and perovskite. Therefore, as shown in Fig. 2h and i, after depositing 1 nm LiF film between PVK and B$_3$PyMpM, compared with original system, the current density is enhanced, and the semicircle radius in the Nyquist plot is reduced, which means that the charge transfer resistance is reduced because the unidirectional enhancement during electron injection process induced by LiF interlayer.

In addition, within our scope of knowledge, LiF has a very large bandgap ($\sim$14 eV [44]). Suppose we simplify the process of electron tunneling through LiF interlayer to the model shown in Fig. S7. In that case, we can find that even though LiF has the property of enhancing charge injection, when the thickness of LiF is large enough, its dielectric property will hinder charge transportation. As shown in Fig. S8, the obstruction of electron (hole) transport by LiF film (8 nm) increases dramatically in single-carrier devices. At the same time, carrier transport is also hindered in PN-type devices rather than the role played by 1 nm LiF interlayer. The decoupling analysis of different types of devices combined with changes in current density and luminance in devices prepared with perovskite nanocrystals of varying chemical composition, as shown in Fig. S9, further supports that the LiF interlayer enhances electron injection and promotes carrier recombination equilibrium.

3.5. The effect of LiF interlayer on injection efficiency, radiative recombination efficiency, and light extraction efficiency

Injection efficiency (*IE*), radiative recombination efficiency (*RE*), and light extraction efficiency (*LEE*) collectively determine the EL performance of PeLEDs, i.e., $EQE = IE \times RE \times LEE$. As shown in Fig. 3d, intrinsic characteristics of perovskite and interlayers on its upper and
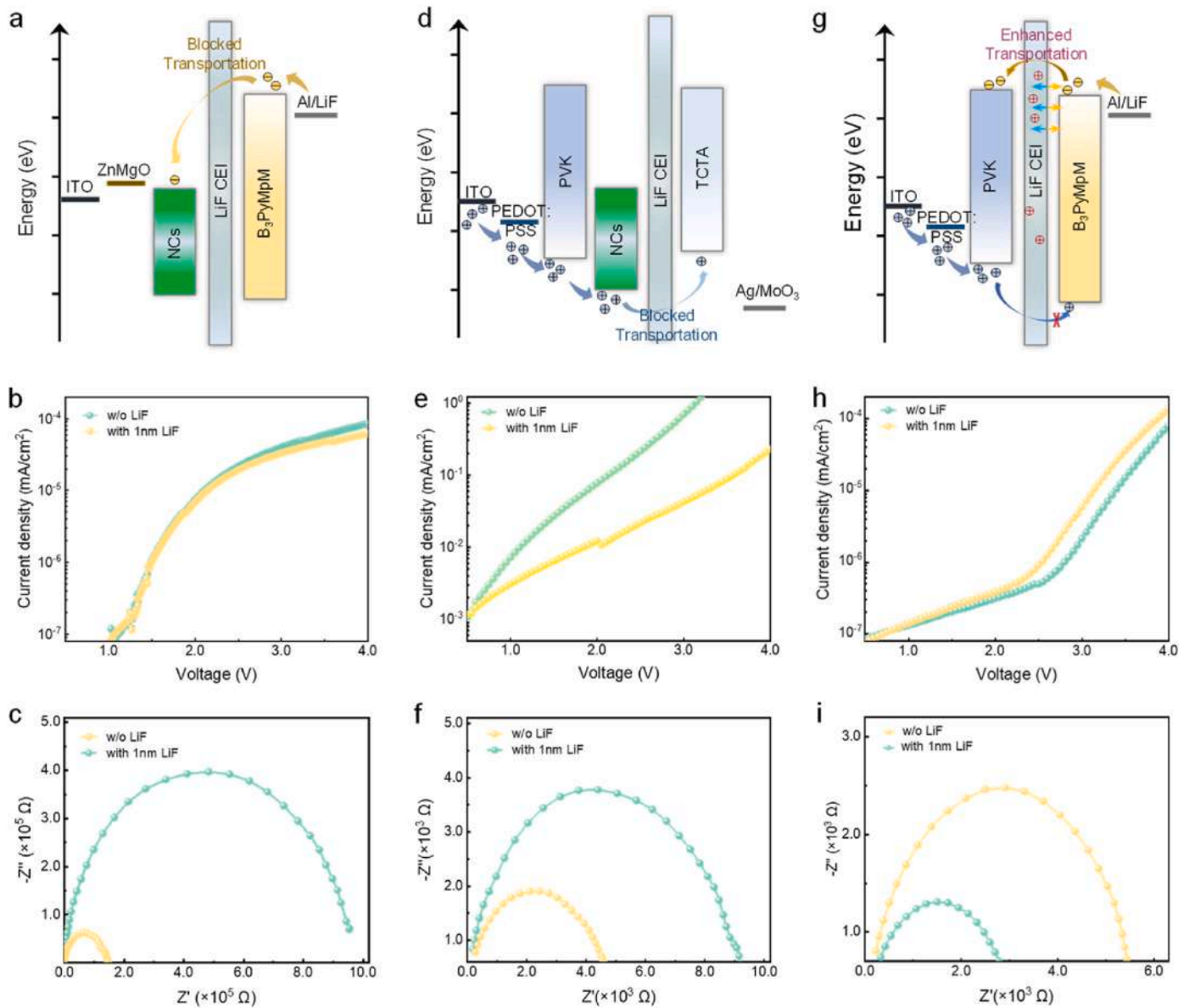
Fig. 2. (a) Schematic of the energy level structure electron-only, (d) hole-only and (g) PN-type devices with the effect of Coulomb-enhanced interlayer on carrier transport. J-V curves of (b) electron-only, (e) hole-only and (h) PN-type devices without and with 1 nm Coulomb-enhanced interlayer. Nyquist plots of (c) electron-only, (f) hole-only and (i) PN-type devices without and with 1 nm Coulomb-enhanced interlayer.

lower surfaces both influence *IE* and *RE* of entire system, and the red region in the middle represents loss mechanisms (non-radiative recombination and parasitic loss) during the carrier injection and recombination processes. As shown in Fig. 3a and b, although the evaporation of LiF on the glass/ITO/PEDOT:PSS/PVK/NCs does not lead to spectral shift, it causes PL quenching and lifetime decay. The same phenomenon is observed after the introduction of LiF on the upper surface of perovskite in glass/ITO/NCs and glass/ITO/PEDOT:PSS/PVK/NCs/B$_3$PyMpM structures, as shown in Fig. S10. The PL quenching and lifetime decay imply the reduction in *RE*, and can be attributed to the high defect density in LiF film grown at high temperature, coupled with its inherent susceptibility to radiation-induced defects formation, contributing to the non-radiative recombination of excitons at the interface when excitation light source irradiates the perovskite in conjunction with the LiF film [32,45].In addition, After evaporation of 1 nm LiF on perovskite, forward and reverse PL tests are carried out. As shown in Fig. S11, there is little difference in PL intensity of the film under different test directions. Combined with the large spectral transparency of LiF itself, it can be

seen that 1 nm LiF has little effect on *LEE*. As we know, in PL testing, the ratio of electrons to holes is typically 1:1, whereas in EL process, the injected charge carriers are often imbalanced [46], as shown in Fig. 3c. Therefore, although the defects in LiF CEI reduce the *RE*, stronger and more balanced charge injection, as shown in Fig. 3d, increases the *IE* and improves the performance of PeLEDs.

3.6. The electroluminescence performance of PeLEDs

The change of carrier transport and recombination processes in PeLEDs can be reflected through the frequency-dependent polarization loss process. With the increase of AC perturbation frequency, the alternating change rate of carrier motion direction increases, resulting in higher frequency oscillation and polarization loss. Therefore, in the control group, the value of dissipation factor-frequency response (the first derivative of dissipation factor of frequency, $\partial D_f/f$) is positive, as shown in Fig. 4a. In the absence of LiF interlayer, holes tend to diffuse from EML to the interface of EML/ETL and recombine. Therefore, as the
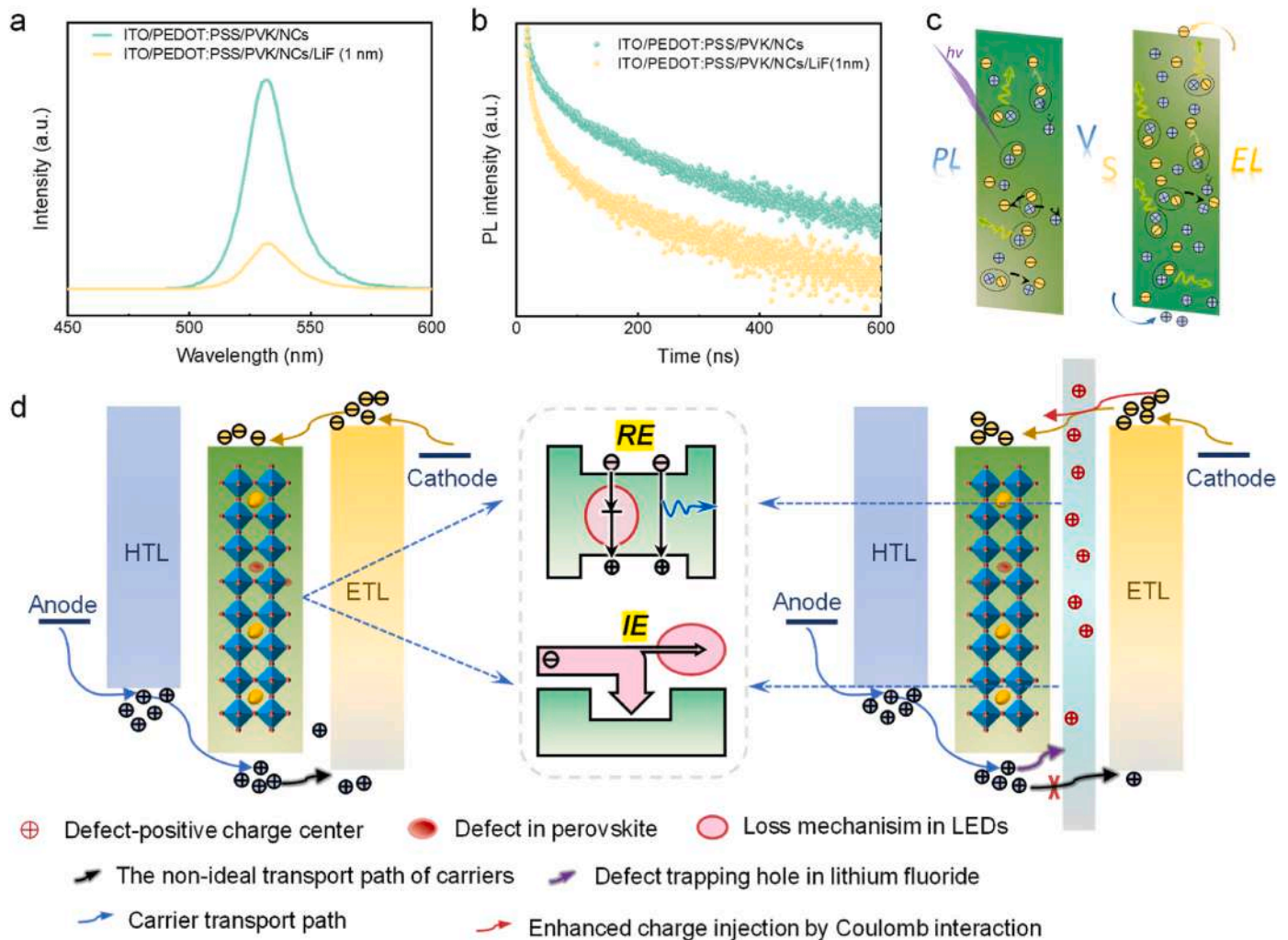
Fig. 3. (a) PL spectra and (b) TRPL spectra of glass/ITO/PEDOT:PSS/PVK/NCs/LiF (0/1 nm). (c) Schematic diagram of the difference in carrier behavior during PL and EL processes. (d) The overall effect of the LiF Coulomb-enhanced interlayer on the surface of perovskite on PeLEDs.

AC perturbation frequency increases, the value of $\partial D_f / f$ in control group changes from monotonically decreasing (from 10^3 Hz to 2×10^4 Hz) to monotonically increasing ($>2 \times 10^4$ Hz). However, as shown in Fig. 4b, due to the characteristics of LiF trapping holes and unidirectional enhancement of electron injection through Coulomb interactions, the value of $\partial D_f / f$ is negative at low frequency and increases monotonically with increasing frequency, and the oscillation phenomenon is shielded. Therefore, in the J-V curves of PeLEDs, as shown in Fig. 4c, the leakage current is lower in devices with LiF CEI when the voltage is below 2.5 V. Meanwhile, the current density in the control group begins to decrease after reaching a maximum value of 173.7 mA/cm² at 8.5 V, due to severe charge accumulation can lead to the deterioration of electroluminescence [47–50] [47–50] [47–50]. The less energy loss induced by the enhanced charge injection and balanced electron-hole recombination leads to the further increase of current density when the voltage is larger than 8.5 V in the devices with 1 nm LiF CEI. Besides, the intensity of EL spectra at 6 V is much higher than that of the control, as shown in Fig. 4d. The peak EQE is also increased from an initial value of 9.9%–18.8%, and the maximum luminance is greatly enhanced from 14379 cd/m² to 82743 cd/m², and the histogram of peak EQE distribution shows that the average peak EQE increased from 11.7% to 15.9% after introducing 1 nm LiF interlayer, as shown in Fig. 4e and f. In addition, as previously analyzed, the thick LiF film(8 nm) will hinder charge transfer, the device current density below 8.5 V is lower than that of the control group, and the Nyquist plot semicircle radius at 4 V is also much

larger, finally reaching a peak EQE of 15.7% and a peak luminance of 49720 cd/m², as shown in Fig. S12.

4. Conclusion

In summary, we have subtly utilized defects to enhance charge injection and balance carrier recombination by introducing 1 nm LiF interlayer between EML and ETL. By combining C–V and multiscale polarization response characterizations, it is confirmed that the defects in LiF films capture holes to form defect-positive charge centers which can attract electrons based on the Coulomb interactions. The EIS and multiscale capacitance response visualize the enhancement of electron injection and the weakening of the carrier accumulation. In further validation, we find that the LiF interlayer only acts as a barrier for carriers due to the absence of holes (electrons) in electron (hole)-only devices, and the electron injection enhancement mechanism remains effective when the interface is constructed in PN-type devices without perovskite. Although the defects in LiF interlayer lead to PL quenching, the increase in injection efficiency improves the EL performance of PeLEDs. The study provides a new perspective on the role of defects and improving the performance of PeLEDs.

CRediT authorship contribution statement

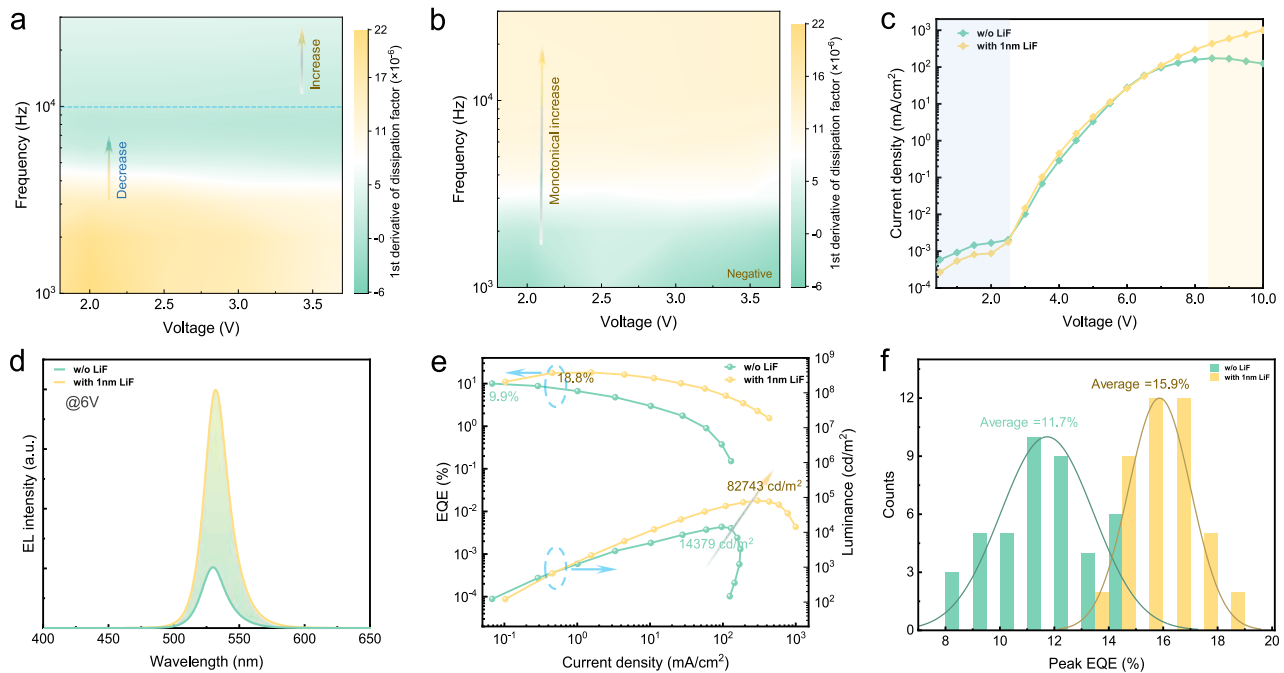**Yongjian Chen:** Writing – review & editing, Writing – original draft,

Fig. 4. The multiscale polarization response of PeLEDs without(a) or with(b) 1 nm LiF interlayer. J-V curves(c), EL spectra(d), EQE-Current density-Luminance curves(c), and Peak EQE count statistics(d) for PeLEDs without or with 1 nm LiF Coulomb-enhanced interlayer.

Methodology, Investigation, Formal analysis, Data curation, Conceptualization. **Cheng Yan:** Writing – review & editing, Supervision, Methodology, Conceptualization. **Zhenyu Chen:** Methodology, Investigation, Conceptualization. **Xiankan Zeng:** Methodology, Conceptualization. **Qungui Wang:** Methodology, Conceptualization. **Shiyu Yang:** Methodology, Conceptualization. **Lunyao Pan:** Methodology, Conceptualization. **Chenglong Li:** Methodology, Conceptualization. **Maolin Mu:** Methodology, Conceptualization. **Guanqi Tang:** Writing – review & editing, Supervision, Methodology, Conceptualization. **Weiqing Yang:** Writing – review & editing, Supervision, Methodology, Funding acquisition, Conceptualization.

Declaration of competing interest

The authors declare that they have no known competing financial interests or personal relationships that could have appeared to influence the work reported in this paper.

Data availability

Data will be made available on request.

Acknowledgments

This work was financially supported by the National Natural Science Foundation of China (Grant No. 52202188), Fundamental Research Funds for the Central Universities(2682023CX063) and China Postdoctoral Science Foundation(2023TQ0048), Postdoctoral Fellowship Program of CPSF(CZC20230375).

Appendix A. Supplementary data

Supplementary data to this article can be found online at https://doi.org/10.1016/j.mtphys.2024.101413.

References

[1] J. Lim, M.T. Hörantner, N. Sakai, J.M. Ball, S. Mahesh, N.K. Noel, Y.-H. Lin, J. B. Patel, D.P. McMeekin, M.B. Johnston, B. Wenger, H.J. Snaith, Elucidating the long-range charge carrier mobility in metal halide perovskite thin films, Energy Environ. Sci. 12 (2019) 169–176.
[2] B. Chen, P.N. Rudd, S. Yang, Y. Yuan, J. Huang, Imperfections and their passivation in halide perovskite solar cells, Chem. Soc. Rev. 48 (2019) 3842–3867.
[3] Y. Zhou, J. Chen, O.M. Bakr, H.-T. Sun, Metal-doped lead halide perovskites: synthesis, properties, and optoelectronic applications, Chem. Mater. 30 (2018) 6589–6613.
[4] S.D. Stranks, H.J. Snaith, Metal-halide perovskites for photovoltaic and light-emitting devices, Nature Nanotech 10 (2015) 391–402.
[5] L.N. Quan, F.P. García De Arquer, R.P. Sabatini, E.H. Sargent, Perovskites for light emission, Adv. Mater. 30 (2018): 1801996.
[6] L.N. Quan, B.P. Rand, R.H. Friend, S.G. Mhaisalkar, T.-W. Lee, E.H. Sargent, Perovskites for next-generation optical sources, Chem. Rev. 119 (2019) 7444–7477.
[7] Z. Chen, Z. Li, C. Zhang, X.-F. Jiang, D. Chen, Q. Xue, M. Liu, S. Su, H.-L. Yip, Y. Cao, Recombination dynamics study on nanostructured perovskite light-emitting devices, Adv. Mater. 30 (2018): 1801370.
[8] M.D. Smith, B.A. Connor, H.I. Karunadasa, Tuning the luminescence of layered halide perovskites, Chem. Rev. 119 (2019) 3104–3139.
[9] J.S. Kim, J.-M. Heo, G.-S. Park, S.-J. Woo, C. Cho, H.J. Yun, D.-H. Kim, J. Park, S.-C. Lee, S.-H. Park, E. Yoon, N.C. Greenham, T.-W. Lee, Ultra-bright, efficient and stable perovskite light-emitting diodes, Nature 611 (2022) 688–694.
[10] Y. Jiang, C. Sun, J. Xu, S. Li, M. Cui, X. Fu, Y. Liu, Y. Liu, H. Wan, K. Wei, T. Zhou, W. Zhang, Y. Yang, J. Yang, C. Qin, S. Gao, J. Pan, Y. Liu, S. Hoogland, E. H. Sargent, J. Chen, M. Yuan, Synthesis-on-substrate of quantum dot solids, Nature 612 (2022) 679–684.
[11] S. Yuan, L. Dai, Y. Sun, F. Auras, Y.-H. Zhou, R.-Z. An, Y. Liu, C. Ding, C. Cassidy, X. Tang, S.-C. Dong, H.-B. Kang, K. Chen, X. Liu, Z.-F. Ye, Y. Zhao, C. Adachi, L.-S. Liao, N.C. Greenham, Y. Qi, S.D. Stranks, L.-S. Cui, R.H. Friend, Efficient blue electroluminescence from reduced-dimensional perovskites, Nat. Photon. (2024), https://doi.org/10.1038/s41566-024-01382-6.
[12] J. Zhang, B. Cai, X. Zhou, F. Yuan, C. Yin, H. Wang, H. Chen, X. Ji, X. Liang, C. Shen, Y. Wang, Z. Ma, J. Qing, Z. Shi, Z. Hu, L. Hou, H. Zeng, S. Bai, F. Gao, Ligand-induced cation-π interactions enable high-efficiency, bright and spectrally stable rec. 2020 pure-red perovskite light-emitting diodes, Adv. Mater. (2023): 2303938.
[13] H. Min, N. Wang, N. Chen, Y. Tong, Y. Wang, J. Wang, J. Liu, S. Wang, X. Wu, P. Yang, H. Shi, C. Zhuo, Q. Chen, J. Li, D. Zhang, X. Lu, C. Zhu, Q. Peng, L. Zhu, J. Chang, W. Huang, J. Wang, Spin coating epitaxial heterodimensional tin perovskites for light-emitting diodes, Nat. Nanotechnol. (2024), https://doi.org/10.1038/s41565-023-01588-9.

[14] W. Zhang, B. Li, C. Chang, F. Chen, Q. Zhang, Q. Lin, L. Wang, J. Yan, F. Wang, Y. Chong, Z. Du, F. Fan, H. Shen, Stable and efficient pure blue quantum-dot LEDs enabled by inserting an anti-oxidation layer, Nat. Commun. 15 (2024) 783.

[15] H.-D. Lee, S.-J. Woo, S. Kim, J. Kim, H. Zhou, S.J. Han, K.Y. Jang, D.-H. Kim, J. Park, S. Yoo, T.-W. Lee, Valley-centre tandem perovskite light-emitting diodes, Nat. Nanotechnol. (2024), https://doi.org/10.1038/s41565-023-01581-2.

[16] Z.-K. Tan, R.S. Moghaddam, M.L. Lai, P. Docampo, R. Higler, F. Deschler, M. Price, A. Sadhanala, L.M. Pazos, D. Credgington, F. Hanusch, T. Bein, H.J. Snaith, R. H. Friend, Bright light-emitting diodes based on organometal halide perovskite, Nature Nanotech 9 (2014) 687–692.

[17] W. Bai, T. Xuan, H. Zhao, H. Dong, X. Cheng, L. Wang, R. Xie, Perovskite light-emitting diodes with an external quantum efficiency exceeding 30, Adv. Mater. 35 (2023): 2302283.

[18] Y. Li, H. Wu, W. Qi, X. Zhou, J. Li, J. Cheng, Y. Zhao, Y. Li, X. Zhang, Passivation of defects in perovskite solar cell: from a chemistry point of view, Nano Energy 77 (2020) 105237.

[19] W. Cao, C. Xiang, Y. Yang, Q. Chen, L. Chen, X. Yan, L. Qian, Highly stable QLEDs with improved hole injection via quantum dot structure tailoring, Nat. Commun. 9 (2018) 2608.

[20] F. So, D. Kondakov, Degradation mechanisms in small-molecule and polymer organic light-emitting diodes, Adv. Mater. 22 (2010) 3762–3777.

[21] C. Coburn, S.R. Forrest, Effects of charge balance and exciton confinement on the operational lifetime of blue phosphorescent organic light-emitting diodes, Phys. Rev. Applied 7 (2017): 041002.

[22] S. Chen, X. Jiang, F. So, Hole injection polymer effect on degradation of organic light-emitting diodes, Org. Electron. 14 (2013) 2518–2522.

[23] L. Zhang, X. Yang, Q. Jiang, P. Wang, Z. Yin, X. Zhang, H. Tan, Y. Yang, M. Wei, B. R. Sutherland, E.H. Sargent, J. You, Ultra-bright and highly efficient inorganic based perovskite light-emitting diodes, Nat. Commun. 8 (2017): 15640.

[24] J. Xing, Y. Zhao, M. Askerka, L.N. Quan, X. Gong, W. Zhao, J. Zhao, H. Tan, G. Long, L. Gao, Z. Yang, O. Voznyy, J. Tang, Z.-H. Lu, Q. Xiong, E.H. Sargent, Color-stable highly luminescent sky-blue perovskite light-emitting diodes, Nat. Commun. 9 (2018) 3541.

[25] P. Schulz, D. Cahen, A. Kahn, Halide perovskites: is it all about the interfaces? Chem. Rev. 119 (2019) 3349–3417.

[26] C. Mai, D. Yu, J. Li, G. Huang, H. Zheng, L. Mu, Y. Cun, J. Wang, G. Xie, J. Wang, J. Peng, Y. Cao, Insulator as efficient hole injection layer in perovskite light-emitting device via MIS contact, Adv. Opt. Mater. 8 (2020): 1902177.

[27] Z. Wang, F. Yuan, W. Sun, H. Shi, T. Hayat, A. Alsaedi, L. Fan, Z. Tan, Multifunctional p-type carbon quantum dots: a novel hole injection layer for high-performance perovskite light-emitting diodes with significantly enhanced stability, Adv. Opt. Mater. 7 (2019) 1901299.

[28] X. Zhang, H. Lin, H. Huang, C. Reckmeier, Y. Zhang, W.C.H. Choy, A.L. Rogach, Enhancing the brightness of cesium lead halide perovskite nanocrystal based green light-emitting devices through the interface engineering with perfluorinated ionomer, Nano Lett. 16 (2016) 1415–1420.

[29] X. Xiao, K. Wang, T. Ye, R. Cai, Z. Ren, D. Wu, X. Qu, J. Sun, S. Ding, X.W. Sun, W. C.H. Choy, Enhanced hole injection assisted by electric dipoles for efficient perovskite light-emitting diodes, Commun Mater 1 (2020) 81.

[30] Q. Zhang, Y. Zhao, X. Qin, M. Li, H. Sun, P. Zhou, W. Feng, Y. Li, J. Lu, K. Lin, L. Shi, Z. Wei, Efficient perovskite light-emitting diodes enabled by nickel acetate interlayer, Adv Funct Materials (2023): 2308547.

[31] T. Okachi, T. Nagase, T. Kobayashi, H. Naito, Influence of injection barrier on the determination of charge-carrier mobility in organic light-emitting diodes by impedance spectroscopy, Thin Solid Films 517 (2008) 1331–1334.

[32] R.M. Montereali, Point defects in thin insulating films of lithium fluoride for optical microsystems, in: Handbook of Thin Films, Elsevier, 2002, pp. 399–431.

[33] C. Yan, X. Zeng, Q. Wang, X. Peng, W. Li, J. Cao, Y. Gao, X. Chu, X. Fu, S. Yang, Y. Chen, W. Yang, Unraveling hole interlayer-dependent interfacial energetics of LEDs, Nano Energy 102 (2022): 107621.

[34] X. Xiao, T. Ye, J. Sun, X. Qu, Z. Ren, D. Wu, S. Ding, X.W. Sun, W.C.H. Choy, K. Wang, Capacitance–voltage characteristics of perovskite light-emitting diodes: modeling and implementing on the analysis of carrier behaviors, Appl. Phys. Lett. 120 (2022): 243501.

[35] H.P. Schwan, Alternating current electrode polarization, Biophysik 3 (2) (1966) 181–201.

[36] H. Liu, T.B. Shonde, F. Gonzalez, O.J. Olasupo, S. Lee, D. Luong, X. Lin, J.S. R. Vellore Winfred, E. Lochner, I. Fatima, K. Hanson, B. Ma, Efficient red light emitting diodes based on a zero-dimensional organic antimony halide hybrid, Adv. Mater. 35 (2023): 2209417.

[37] X. Zeng, C. Yan, Q. Wang, X. Fu, S. Yang, Y. Chen, L. Pan, W. Li, W. Yang, High curvature PEDOT:PSS transport layer toward enhanced perovskite light-emitting diodes, Small (2023): 2304411.

[38] M.-L. Guo, Y. Lu, X.-Y. Cai, Y. Shen, X.-Y. Qian, H. Ren, Y.-Q. Li, W.-J. Wang, J.-X. Tang, Interface engineering improves the performance of green perovskite light-emitting diodes, J. Mater. Chem. C 10 (2022) 2998–3005.

[39] L. Zhang, D. Taguchi, H. Masada, T. Manaka, M. Iwamoto, Channel formation as an interface charging process in a pentacene field effect transistor investigated by time-resolved second harmonic generation and impedance spectroscopy, Jpn. J. Appl. Phys. 51 (2012): 02BK08.

[40] L. Zhang, D. Taguchi, J. Li, T. Manaka, M. Iwamoto, Transport limited interfacial carrier relaxation in a double-layer device investigated by time-resolved second harmonic generation and impedance spectroscopy, Appl. Phys. Lett. 98 (2011): 092109.

[41] J. Jamnik, J. Maier, Treatment of the impedance of mixed conductors equivalent circuit model and explicit approximate solutions, J. Electrochem. Soc. 146 (1999) 4183–4188.

[42] M. Bag, L.A. Renna, R.Y. Adhikari, S. Karak, F. Liu, P.M. Lahti, T.P. Russell, M. T. Tuominen, D. Venkataraman, Kinetics of ion transport in perovskite active layers and its implications for active layer stability, J. Am. Chem. Soc. 137 (2015) 13130–13137.

[43] M. Kazes, T. Udayabhaskararao, S. Dey, D. Oron, Effect of surface ligands in perovskite nanocrystals: extending in and reaching out, Acc. Chem. Res. 54 (2021) 1409–1418.

[44] D.B. Sirdeshmukh, L. Sirdeshmukh, K.G. Subhadra, Alkali Halides: A Handbook of Physical Properties, Springer Berlin Heidelberg, Berlin, Heidelberg, 2001.

[45] B.F. Bory, H.L. Gomes, R.A.J. Janssen, D.M. De Leeuw, S.C.J. Meskers, Electrical conduction of LiF interlayers in organic diodes, J. Appl. Phys. 117 (2015): 155502.

[46] S.D. Stranks, R.L.Z. Hoye, D. Di, R.H. Friend, F. Deschler, The physics of light emission in halide perovskite devices, Adv. Mater. 31 (2019): 1803336.

[47] T.-H. Han, W. Song, T.-W. Lee, Elucidating the crucial role of hole injection layer in degradation of organic light-emitting diodes, ACS Appl. Mater. Interfaces 7 (2015) 3117–3125.

[48] D. Zhang, D. Zhang, L. Duan, Exploiting p-type delayed fluorescence in hybrid white OLEDs: breaking the trade-off between high device efficiency and long lifetime, ACS Appl. Mater. Interfaces 8 (2016) 23197–23203.

[49] B. Liu, M. Xu, L. Wang, Y. Su, D. Gao, H. Tao, L. Lan, J. Zou, J. Peng, High-performance hybrid white organic light-emitting diodes comprising ultrathin blue and orange emissive layers, Appl. Phys. Express 6 (2013): 122101.

[50] D. Zhang, L. Duan, Y. Zhang, M. Cai, D. Zhang, Y. Qiu, Highly efficient hybrid warm white organic light-emitting diodes using a blue thermally activated delayed fluorescence emitter: exploiting the external heavy-atom effect, Light Sci. Appl. 4 (2015) e232–e232.